Applied Catalysis B: Environmental 343 (2024) 123580

Contents lists available at ScienceDirect

Applied Catalysis B: Environmental

journal homepage: www.elsevier.com/locate/apcatb

Iron phthalocyanine hollow architecture enabled ammonia production via nitrate reduction to achieve 100 % Faradaic efficiency

Sougata Sarkar [a], Ashadul Adalder [a], Sourav Paul [a], Samadhan Kapse [b], Ranjit Thapa [b], Uttam Kumar Ghorai [a,*]

[a] Department of Industrial Chemistry & Applied Chemistry, Swami Vivekananda Research Centre, Ramakrishna Mission Vidyamandira, Belur Math, Howrah 711202, India

[b] Department of Physics and Centre for Computational and Integrative Sciences, SRM University – AP, Amaravati, Andhra Pradesh 522240, India

ARTICLE INFO

Keywords:
Iron phthalocyanine
Green ammonia
Nitrate reduction
Electrocatalyst
Haber–Bosch process

ABSTRACT

Eight electron nitrate (NO_3^-) reduction to ammonia (NH_3) offers a cost–effective and energy efficient route than the Haber–Bosch process. The state of art electrocatalysts for nitrate reduction shows potential activity, albeit suffering from poor Faradaic efficiency, kinetically sluggish multi electron–proton process, and competitive hydrogen evolution reaction. Herein, we present a hollow iron phthalocyanine (FePc) rectangular nanotube (RNTs) electrocatalyst with 100 % Faradaic efficiency and 35067.09 μg h^{-1} mg_{cat}^{-1} ammonia yield, which is 3.5 times higher than that of FePc nanorods. One-of-a-kind hollow nanostructure has Fe-N_4 active motif sites necessary for NO_3^- activation, dissociation, specific intermediate formation, and interaction, resulting in the energy-efficient generation of NH_3, according to in-situ research combined with theoretical analysis of molecular scale reaction mechanism. These unique results, coupled with the monitoring of pH changes in real time during electrolysis, open up new possibilities for progressive ammonia production with reduced carbon footprint.

1. Introduction

Ammonia (NH_3) is a fundamental component of nitrogen fertilizers and considered as an environmentally friendly, hydrogen-rich, yet carbon-free fuel in the industrial sector [1]. The Haber–Bosch process can only produce ammonia on a large scale, where nitrogen and hydrogen react using iron-based catalyst under extreme circumstances of high temperature (400–600 °C) and pressure (200–350 atm). The annual production of NH_3 is 150 million tonnes via Haber–Bosch process results in a significant energy consumption and accelerates environmental catastrophe [2–4]. Alternately, electrocatalytic N_2-to-NH_3 conversion has recently received due to its hospitable environment and compatibility with renewable electricity, it has generated scientific interest. This conversion involves employing water as proton source [5–13]. The intrinsic properties of nitrogen that is low water solubility and high N≡N bond dissociation energy (941 kJ mol^{-1}) result in insufficient selectivity and yield rates of the N_2-to-NH_3 process that are significantly lower than the Haber-Bosch process [14–18]. As an alternate and low-temperature ammonia production method is an urgent need, the electrochemical reduction of nitrate (NO_3RR) to NH_3 ($NO_3^- + 6H_2O + 8e^- \rightarrow NH_3 + 9OH^-$) offers the following benefits [19–22]: (i) Compared to the Haber-Bosch process and NRR, dissociation of N = O (in NO_3^-) uses far less energy (204 kJ mol^{-1}), making NO_3RR an energy-efficient process. (ii) As nitrate is prevalent in both industrial waste and agricultural runoff, widespread production of NO_3RR is possible. (iii) NO_3^- ions are highly soluble in water (880 g/L) while N_2 has very low solubility (0.02 g/L) [23], hence, NO_3^- ions will be adsorbed at the surface on the catalyst more efficiently than N_2, resulting in higher electrocatalytic performance. The hydrogen evolution reaction (HER) potential (0 V vs RHE), is frequently below the potential of NO_3^- to NH_3, which results in poor Faradaic efficiency. Therefore, it is desirable to develop catalysts that can only turn NH_3 from NO_3^- while suppressing HER [24,25]. Several attempts were taken to develop transition metals [21,26–30], alloys & compounds [31–38] and composites [39–47] for NO_3RR. It is significant to remember that the formation of metal-H bonds is aided by d orbital electrons in transition metals with appropriate symmetry. In consequence, this causes a decrease in the catalytic efficiency of NO_3RR process while also increasing the competitive HER [27]. As a result, introduccing a non-metallic equivalent into the transition metal compound may provide a method for reducing the

* Corresponding author.
E-mail address: uttam.indchem@vidyamandira.ac.in (U.K. Ghorai).

https://doi.org/10.1016/j.apcatb.2023.123580
Received 9 September 2023; Received in revised form 24 November 2023; Accepted 27 November 2023
Available online 29 November 2023

adsorption capacity of hydrogen to the complex while inhibiting the HER [24]. Another perspective is that many valence electrons in non-metallic components provide additional support for NO_3RR. Recently, Zhang et al. [48] developed the iron-based, ordered mesoporous carbon framework structure and studied the role of mesochannels in electrocatalytic performance. In the recent studies, we have identified various actives sites (like Cu/Co/Ni, carbon atom close to the pyridinic N1, pyrrolic-N, and pyridinic-N2) in transition metal phthalocyanine nanostructures such as copper phthalocyanine, cobalt phthalocyanine, and nickel phthalocyanine, etc. for nitrogen and carbon dioxide fixation [9,18,49–51]. Therefore, designing and discovering the NO_3RR electrocatalytic activities of FePc hollow nanostructures for NH_3 production under ambient condition is truly challenging. However, to the best of our knowledge, there has been no study on FePc RNTs for the electrocatalytic NO_3RR.

Inspired by the above discussion, herein we have designed and developed a unique novel rod and hollow FePc nanotubes possessing Fe-N_4 active centre for e-NO_3RR to NH_3 in normal circumstances. Nanorods are nanostructures with an elongated, rod-like shape. FePc nanorods are rectangular in shape and are often tailored for their unique properties and suitability for certain reactions. Also, the unique geometry of the FePc hollow nanotubes allows the inside surface of the nanotubes to electrocatalytically react with the nitrates, which can produce essential chemical intermediates. As a consequence, the catalyst exhibits high NH_3 yield with maximum FE at −1.5 V vs RHE are 35067.09 μg h^{-1} mg_{cat}^{-1} and 100 % respectively during NO_3RR. The Fe center's local coordination environment around the pyrrolic and pyridinic N in FePc RNTs is illustrated by the X-ray absorption fine structures (XAFS). As the exothermic and endothermic adsorption behaviors of NO_3 and H, respectively, the theoretical investigation analysis shows that the Fe center surrounding the pyridinic nitrogen is the predominant active site to capture the NO_3 molecule for e-NO_3RR in comparison to HER. This study exhibits the concept of amalgamating precisely synthesized nanotubes and computation guided mechanism of vital interaction of the reaction intermediates with active sites, overcome the limitation of electrocatalytic performance, and foster advancement in the ammonia production technology by the low–carbon strategy.

2. Experimental section

2.1. Synthesis of FePc RNTs

Utilising commercially available compounds, the FePc was synthesised. 1.44 mmol of iron (II) acetate (Sigma-Aldrich), 5.76 mmol of phthalonitrile (Sigma-Aldrich), and 30 mg of ammonium heptamolybdate tetrahydrate (Merck) catalyst were taken into ethylene glycol solvent. The mixture was placed into a 100 mL autoclave coated with Teflon after 30 min of stirring at 60 °C. After that, the autoclave was put into an oven and kept at 180 °C for 24 h. The precipitate was repeatedly washed with hot 1.0 M HCl and ethanol to eliminate any byproducts after cooling to room temperature. Finally, the produced FePc RNTs were dried for 12 h in a vacuum oven at 65 °C.

The same procedure for the synthesis of FePc nanorods was maintained (as in the preparation of FePc RNTs) with a change to an autoclave in the oven at 120 °C for 6 h.

2.2. Characterizations technique and electrochemical set–up

Using a Bruker D-8 advanced Eco X-ray powder diffractometer apparatus, the crystal structure and phase identification of iron phthalocyanine (FePc) were validated by X-ray diffraction technique (XRD). In the XRD technique, a monochromatic radiation of Cu-K_α (wavelength, = 0.15404 nm) was utilised, and a voltage of 40 kV and a current of 25 mA were used, respectively, to preserve the optimum equilibrium conditions. Using a Shimadzu UV-3600 Plus UV–vis spectrophotometer, the quantity of ammonia was measured. The CHI 760E electrochemical instrument, which has a three-electrode system with a platinum (Pt) foil acting as the counter electrode, Ag/AgCl (in 3.5 M KCl) acting as the reference electrode, and carbon paper loaded with FePc catalyst ink acting as the working electrode, was used for all the measurements involving electro-catalytic reduction of nitrate to synthesise ammonia. The reversible hydrogen electrode (RHE) was used to accurately convert every potential reading. The entire electrochemical process was carried out in an H-type cell.

2.3. Electrocatalytic nitrate reduction performance of FePc

All electrocatalytic nitrate reduction experiments were performed in CHI 760E workstation using 0.1 M K_2SO_4 with 0.5 M KNO_3 solution in an H–type electrochemical cell (Fig. S3) where anode and cathode chamber were separated by a Nafion 117 membrane under ambient condition. Nafion membrane was pre-treated with 5 % H_2O_2 solution, 0.05 M H_2SO_4 solution, and ultrapure water prior to use. To investigate the electrocatalytic nitrate reduction activity on FePc RNT electrocatalysts, linear sweep voltammetry (LSV) was performed on carbon paper (CP) electrodes with scan rate of 100 mV/s.

2.4. FePc ink preparation

20 mg FePc was accurately weighted and was taken in a vial, then dispersed with 900 μL iso-propanol (Merck) solution. After few minutes of sonication, 100 μL Nafion 117 (5 wt %) (Sigma-Aldrich) solution was poured into the solution. Finally, the prepared mixture was shaken in vortex machine for 10 mins to make it homogeneous and useable ink was prepared for further use. Then the 50 μL prepared ink was loaded on a 1 × 1 cm^2 carbon paper.

2.5. Determination of ammonia yield rate and FE

Using UV–vis spectrophotometer the quantity of ammonia was measured by indophenol blue method [9]. During experiment, 2 mL of coloring solution (1 M sodium hydroxide solution containing 5 wt % trisodium citrate dihydrate and 5 wt % salicylic acid (Merck Co., Ltd.)), 1 mL of oxidizing solution (0.05 M sodium hypochlorite solution (4 % w/v available chlorine) (Merck Co., Ltd.)) and 0.2 mL of catalyst solution (1.01 g (3.34 mmol) sodium nitroprusside dihydrate (Loba Chemie Co., Ltd)) were added to 2 mL of certain dilutated electrolyte solution (was taken from the electrolytic cell after NO_3RR). Then the resulting solution was incubated at room temperature for two hours, and analysed spectrophotometrically. The analysed absorption spectrum showed maximum absorbance at 660 nm, indicating the formation of indophenol in the mixture, which confirmed the formation of ammonia during NO_3RR. For the calibration purpose, ammonium ion (ammonium chloride, Merck) solution was used with varying the concentration, {0.0, 0.2, 0.4, 0.6, 0.8, 1.0 (μg/mL)} in 0.1 M K_2SO_4 solution. From the Fig. S7, the fitting curve ($y = 0.20136\,x + 0.02727$; $R^2 = 0.999$) showed an optimized linear relationship between absorbance and concentration of ammonia, after three repeated calibrations.

The following equations were used to compute the ammonia yield rate and the faradic efficiency following the electrochemical reduction of NO_3^- to ammonia:

$$\text{Ammoniayieldrate} = \frac{(C_{NH_3} x V)}{(m_{cat} x t)} \quad (1)$$

$$FE\left(\%\right) = \frac{(8 \times F \times C_{NH_3} \times V)}{(17 \times Q)} x100\% \quad (2)$$

In this equation, $C_{ammonia}$ is the concentration of ammonia created after the electrochemical reduction of NO_3^-, V is the total volume of electrolyte used, t is the amount of time needed for the reduction process, m is the mass of the catalyst, F is the Faraday constant

(96,485 C mol^{-1}), and Q is the total charge moving through the electrode.

Amount of nitrate conversion is calculated by the given equation:

$$\text{Conversion}\left(\%\right) = \frac{\Delta C_{NO_3^-}}{C^0_{NO_3^-}} x100\% \quad (3)$$

Where, $C^0_{NO_3^-}$ is the initial nitrate concentration in the electrolyte solution and $\Delta C_{NO_3^-}$ is nitrate concentration difference before and after the electroreduction process.

The energy efficiency of half cell for ammonia is calculated by the equation [26]:

$$EE\left(\%\right) = \frac{\left(1.23 - E^0_{NH_3}\right) xFE_{NH_3}}{(1.23 - E)} x100\% \quad (4)$$

Where, EE is energy efficiency. Assuming the overpotential of anodic electrode for water oxidation is zero. E^0 (NH_3) is 0.69 V for nitrate reduction and the equilibrium potential for water oxidation is 1.23 V.

2.6. Isotope labelling experiments by ^{1}H NMR method

Using a 0.5 M solution of $K^{15}NO_3$ (98 atom % ^{15}N Sigma-Aldrich Co.) as the nitrogenous source, the electrochemically produced $^{15}NH_3$ was confirmed by an isotope-labelled tracer experiment. The composition of the electrolyte solution of $^{15}NH_4^+$ after an electrocatalytic nitrate reduction reaction for one hour was investigated using ^{1}H NMR (600 MHz) spectroscopy using D_2O as an internal standard solution.

3. Results and discussion

3.1. Catalyst synthesis and characterization

The FePc RNTs were synthesised by solvothermal strategy. The cyano group of phthalonitrile undergoes a nucleophilic attack by ethylene glycol, which results in the development of 1-(2-hydroxyethoxy)-3-iminoisoindolenine intermediate (Fig. 1a). Subsequently, Fe^{2+} cation undergoes cyclization using four intermediate systems generating one FePc RNTs unit, which then undergoes π-π interaction with each other in a parallel fashion to form FePc RNTs half tubular structures, which in turn produce complete rectangular tubular structures (Fig. 1b). FePc is a square planar complex in which the ligands and the core metal ion (Fe) are covalently bound by pyrrolic nitrogen centres. The crystal field splitting of Fe d orbitals in FePc [52–54] shown in Fig. 1c. We propose that by tuning the interactions between the Fe center of FePc and nitrates would enhance NO_3RR. Since the oxygen in nitrate ions can donate an electron pair to the metal centre, forming a σ bond, and the antibonding orbital (π *) of the nitrate group (N–O bond) can also accept an electron pair by back bonding from the filled d orbitals of the metal centre, thereby polarising and ultimately reducing the nitrate ions. This synergistic effect facilitates attachment of the nitrate ions to the active site (metal centre) of the catalyst system (Fig. 1c).

Fig. 2a displays the XRD pattern to investigate the crystallinity and phase identification of FePc RNTs. The FePc RNTs crystal features a monoclinic crystal system with the space group $^P2_{1/c}$, and the two prominent peaks at 7° and 9.2° signify the crystal's phase development. The entire XRD pattern indexed as (100), ($\bar{1}$02), (002), ($\bar{2}$02), (200) (102), ($\bar{3}$02), ($\bar{1}$04) corresponds well with the JCPDS card number 14–0926. The chemical bonding of FePc RNTs is further investigated by

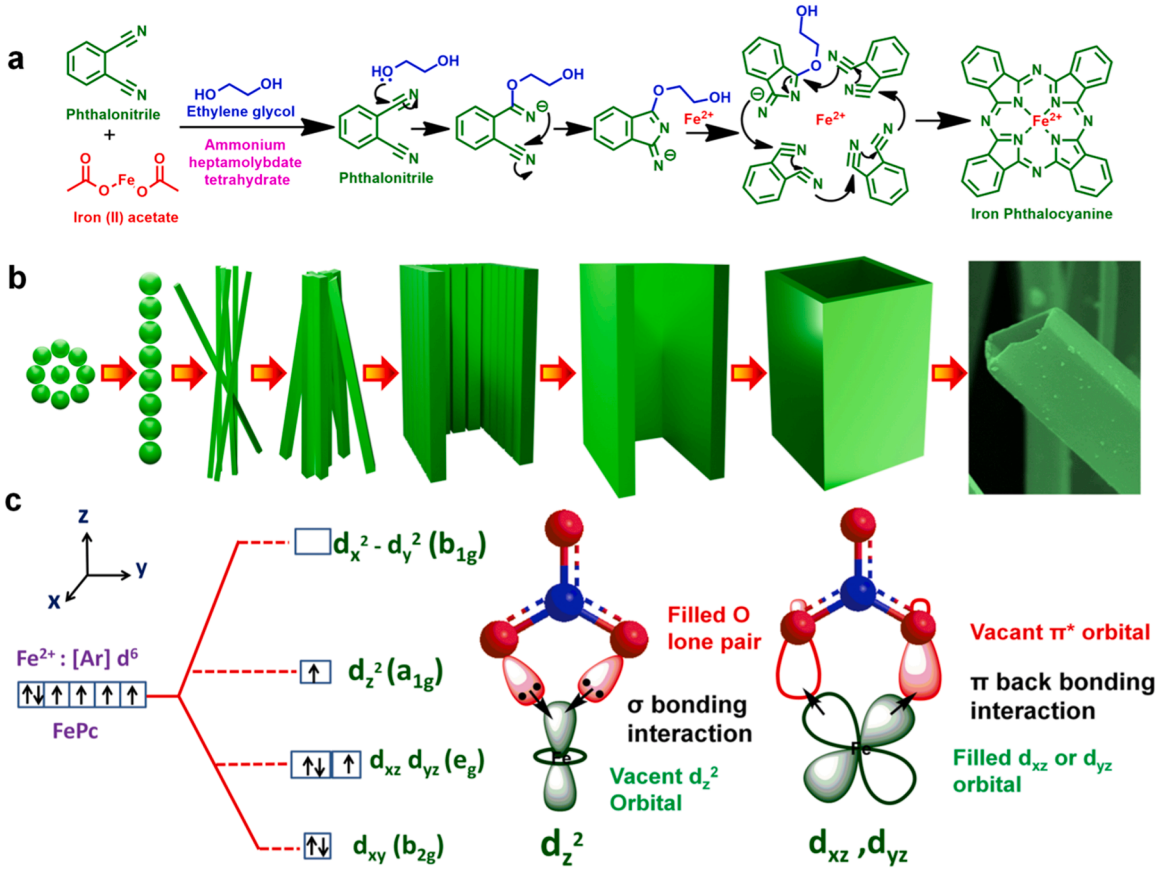

Fig. 1. (a) Mechanism for the synthesis of the FePc molecule; (b) Growth mechanism for FePc RNTs; (c) Iron(II) phthalocyanine electronic ground state and orbital interaction of metal d orbital with NO_3^-.

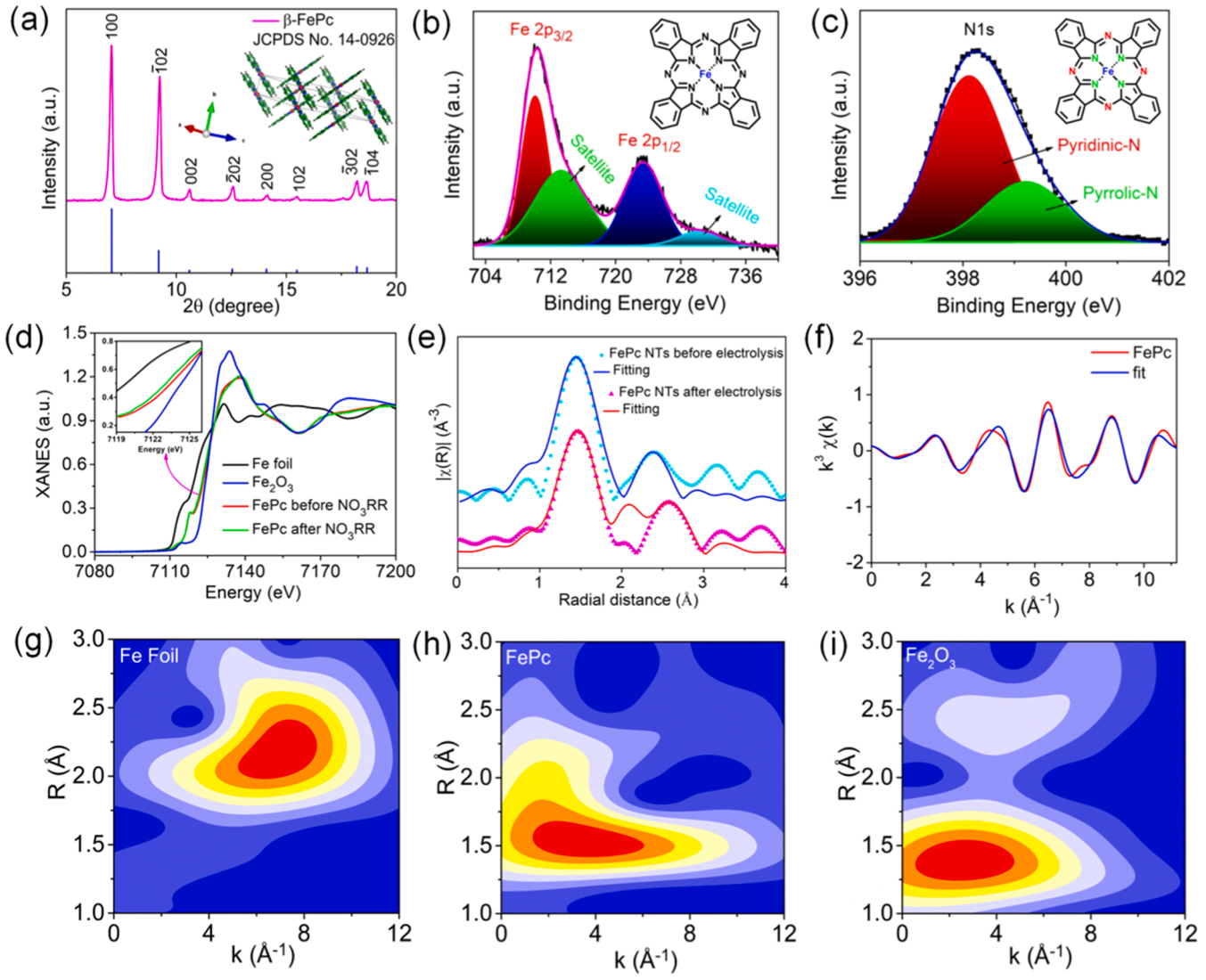

Fig. 2. (a) XRD pattern of FePc RNTs, (b–c) high resolution XPS spectra of Fe 2p doublet and N 1 s respectively, (d) Normalized XANES spectra at Fe K-edge; (e) Experimental $\chi(R)$ vs.R data of FePc RNTs measured at Fe K-edge; (f) EXAFS fitting curves in k space; (g-i) WT of Fe foil, FePc, and Fe_2O_3, respectively.

spectroscopic study (Fig. S1 and Fig. S2). The valence state and chemical makeup of FePc were investigated using an XPS experiment. The 710.1 eV and 723.37 eV peaks in Fig. 2**b** are attributed to the electronic states of Fe $2p_{3/2}$ and $2p_{1/2}$ respectively [55]. The two satellite peaks at 713.1 eV and 730.2 eV represents the divalent state of Fe in the FePc molecule. A high resolution spectra of N1s is shown in Fig. 2c. It has two peaks at 398.1 eV and 399.2 eV that correspond to the pyridinic nitrogen group and the pyrrolic nitrogen group in the FePc molecule, respectively. The central Fe atom is connected to this pyrrolic nitrogen atom, and the carbon atom is bonded to the pyridinic nitrogen atoms.

Utilising synchrotron-based extended X-ray absorption fine structure (EXAFS) and X-ray absorption near-edge structure (XANES) investigations, it was determined what valence state(s) and local coordination environment(s) iron in the FePc RNTs electrocatalyst was in both during and before the NO_3RR process. Fig. 2d shows Fe-K-edge normalized XANES spectra of Fe foil, Fe_2O_3, and FePc NTs (before and after electrolysis), at a potential of −1.5 V vs RHE. For FePc samples, Fe-K-edge lies in between Fe foil and Fe_2O_3, refers that FePc have oxidation states spanning from 0 to +3 [26,56,57]. A pre-edge peak around 7118 eV can be inferred to the square-planar, centrosymmetric Fe-N_4 structure of FePc RNTs. In Fig. 2e, main two distinct peaks can be seen in the quantitative fitting of the FePc RNTs samples' Fourier transformed k^2-weighted EXAFS (FT-EXAFS) spectra (before and after electrolysis). The first peak is at 1.5 Å, corresponding to iron-pyrrolic nitrogen [Fe-N (pyrrolic)] with co-ordination number (CN) 4. (Table S2, Supporting Information), the second peak at 2.5 Å contributions from single scattering C shell with CN 8. The wavelet transform (WT) of Fe K-edge EXAFS oscillations was used to further investigate the atomic dispersion of Fe in FePc because of the strong resolutions in both k and R spaces (Fig. 2f). In the WT contour plots, there is just one intensity maximum that can be seen, and it corresponds to the Fe-N coordination at ~4.6 $Å^{-1}$ [56]. When compared to the WT plots of Fe foil and Fe_2O_3, no intensity maximum attributable to the Fe-Fe contribution can be seen. (Fig. 2g–i). The WT contour plots present a visual image of the existence of various bonds and analyze the variation in co–ordination environment of Fe in FePc and the reference samples (Fe, Fe_2O_3). The intensity maxima correspond to the Fe–N (pyrrolic) coordination and in FePc. With respect to the WT contour plots of Fe foil and Fe_2O_3 Fig. 2g-i, FePc did not show any maxima corresponding to Fe–Fe bonds in the R range from 0 to 3 Å.

The surface morphology of the FePc RNTs was studied as shown in Fig. 3. The results revealed that the FePc RNTs exhibited well-distributed rectangular micro–dimensional nanotubes, mouth section of the tubes are clearly hollow as shown in Fig. 3 a–c (FE-SEM images) but in case of FePc it shown a nano rod like morphology (Fig. S4).

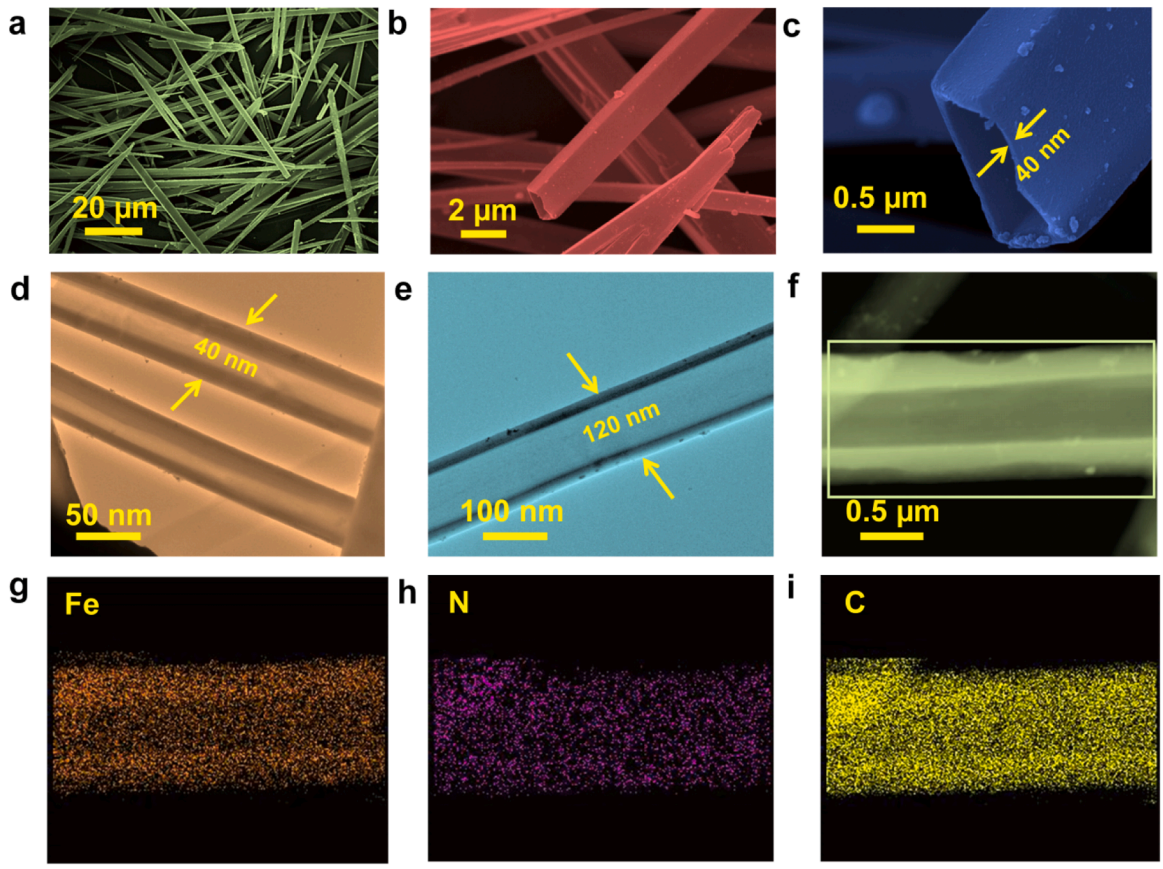

Fig. 3. (a–b) FESEM image of FePc RNTs at different magnification; (c) FESEM image of FePc RNTs having clearly visible rectangular in shape; (d-e) TEM image of hollow FePc RNTs in different magnification; (f) HAADF-STEM image of FePc; (g-i) Elemental distribution of Fe, N and C in FePc RNT.

Furthermore, the distinctive hollow nature of the tubes are established from the TEM image (Fig. 3d–e), which shows that inner section of the tube are vacant. The length of the tube varies from ~30–50 μm (Fig. 3a), while the width ranges from ~ 100–150 nm (Fig. 3d, e), and it has a wall thickness of ~40 nm (Fig. 3**c**). The TEM–EDS mapping of the tube is shown in (Fig. 3**f–i**), the analysis confirmed that Fe, N, and C was present in the synthesized nanotubes.

3.2. Eelectrocatalytic performance of the catalyst

Fig. S5 demonstrates chronoamperometry curves (j vs. t) at various applied potentials of nitrate-containing electrolyte (0.1 M K_2SO_4 + 0.5 M KNO_3) using FePc RNT with minimal fluctuations, indicating stable nature of the catalyst. After chronoamperometry tests the ammonia yield was quantified by indophenol blue method. The UV analysis shows that maximum absorbance (Fig. S8) at ~660 nm confirms the formation of ammonia. The maximum NH_3 yield rate and FE of FePc RNT at −1.5 V were 35067.09 μg h^{-1} mg_{cat}^{-1} and FE 100 %, respectively (Fig. 4a-b). In case of FePc rectangular nanorods (RNR) the obtained maximum NH_3 yield rate and maximum FE at −1.5 V were 11740.71 μg h^{-1} mg_{cat}^{-1} and FE 73.02 %, respectively (Fig. S10). The high ammonia yield rate and Faradaic efficiency values of FePc RNTs are comparable to previously reported data for various transition metal based electrocatalysts such as Fe SAC[27], Fe-PPy SAC[26], Fe_3C nanoflakes[58], FeOOH Nanorod[33], Iron-Cyano Nanosheets[59]. The conversion of nitrate concentration in the electrolyte solution during NO_3RR is important to produce the ammonia and 23.6 % nitrate ion conversion for 1 h was shown at −1.5 V on the FePc electrocatalyst as shown in Fig. 4c. Energy efficiency (EE) was calculated at different potentials using Eq. 4. The EE value for the FePc electrocatalyst was shown to be 19.79 % (Fig. 4d), after electrolysis at −1.5 V for 1 h. Fig. S13 (comparison of UV-Vis & IC study) confirmed that the maximum ammonia yield observed at −1.5 V vs. RHE is comparable with two different methods and instruments.

3.3. Effect of nanotube's distinctive hollow structure on ammonia yield

A probable mechanism for the conversion of nitrate to ammonia from the morphological perspective are presented, in the case of nanorods only outer surface participates in the reduction reaction, while both the inner and outer surface of the hollow nanotube effectively takes part in the electrocatalytic reaction (Fig. 4e-f) FePc nanotube demonstrates morphological and structural superiority over FePc nanorod.

The nanotube hollow structural framework shows the following distinct features which enhances the conversion of nitrate to ammonia. (1) The hollow structure provides binding strength for selective electrochemical ammonia synthesis. (2) The hydrodynamic radius of nitrate ions is 0.2 nm [60], while the width of the tube is ~120 nm, hence nitrate ions can easily enter into the nanotube, as the width of the nanotube is almost 600 times larger than the hydrodynamic radius of nitrate ion. (3) The time of residence of nitrate ions inside the FePc nanotube is quiet high, as the length of the tube is around 30–50 μm, (4) As compared to the nanorod, nanotube contains greater number of exposed active sites as both the external as well as inner surface participates in the electrocatalytic reduction reaction while in case of nanorod only the external surface participates, (5) The additive effect of higher retention time of nitrate ions in nanotube along with greater number of active sites, results in an increase in possibility of conversion of the key intermediates of NO_3^- to NH_3 due to the vital interaction of reaction intermediates with electrocatalytic active sites, hence FePc nanotube exhibits higher ammonia yield as compared to FePc nanorod.

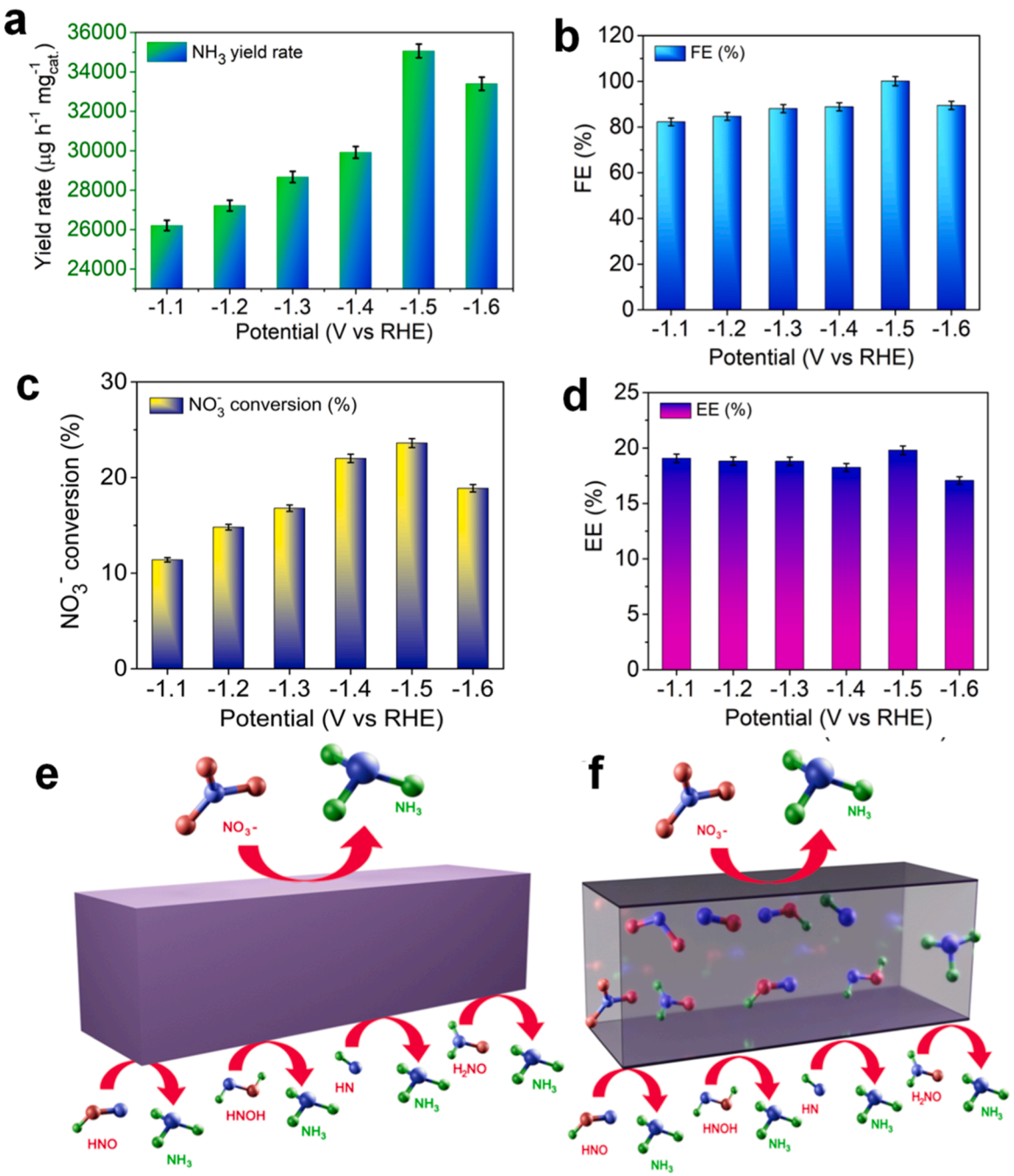

Fig. 4. (a-b) Bar chart of average NH_3 yield rate and corresponding Faradaic efficiency of FePc RNTs at different potential; (c) Bar chart of nitrate conversion at different potential for 1 h; (d) Bar chart of EE at different potential after 1 h electrolysis; (e–f) A schematic figure for nanorods vs nanotubes comparison for nitrate reduction.

3.4. FTIR analysis, different confirmative analysis and catalyst stability analysis

ATR-FTIR is used to track the reaction intermediates during the NO_3RR process from −1.1 V to − 1.6 V. As shown in Fig. 5a, the positive band at ~1389 cm^{-1} is assigned to NO_3^- for while the negative bands correspond to deoxidation intermediates *NO at ~1620 cm^{-1} and 1688 cm^{-1} and for protonation intermediates *NH at ~1340 cm^{-1}, $*NH_2$ at ~1102 cm^{-1} and $*NH_3$ at ~1526 cm^{-1}. The slightly band observed at 1651 cm^{-1} is due to the O–H bending of water present in electrolyte [39,61,62]. To verify the source of ammonia production, an isotope tracing experiment was carried out at a potential of −1.5 V (vs RHE, Fig. 5b). ^1H nuclear magnetic resonance (^1H NMR) spectroscopy was used to identify the ammonia as produced in the electrolyte solution. A doublet peak of $^{15}NH_3$ was obtained when $^{15}NO_3^-$ was used for electrolysis and a triplet peak of $^{14}NH_3$ was obtained when $^{14}NO_3^-$ was used. However no peaks were observed when the experiment was carried out without nitrate in electrolyte. This result further confirms the selective electrochemical nitrate reduction to ammonia by FePc. We have done the several control experiments to confirm the ammonia is actually coming from nitrate solution and not by any others contaminants. In Fig. 5c, after the electroreduction process, a negligible amount of ammonia was produced during "without nitrate solution" and "OCP" test but in the presence of nitrate solution, a measurable amount of ammonia was detected which confirms that ammonia was actually produced from the NO_3RR process. To test the long-term stability of the

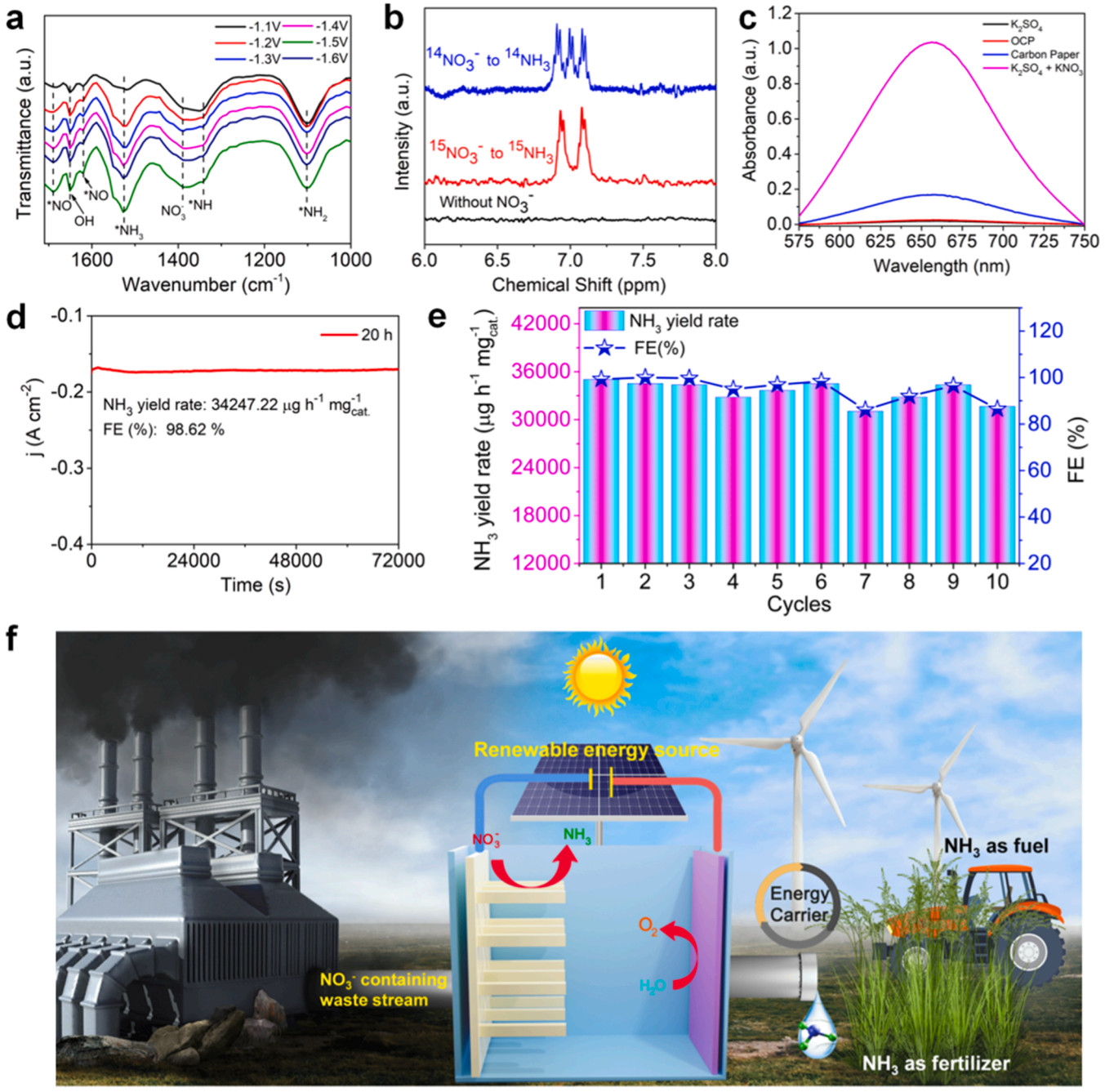

Fig. 5. (a) Potential-dependent ATR-FTIR spectra during the NO_3RR electrolysis; (b) Isotopic labeling experiment with $^{14}NO_3^-$, $^{15}NO_3^-$, and without NO_3^- containing electrolyte solution; (c) Control experiments with CP, OCP, and nitrate with & without electrolyte solution experiment; (d) 20 h durability test for FePc RNTs towards NO_3RR at −1.5 V vs. RHE in nitrate saturated electrolyte; (e) Recycling stability tests of FePc RNTs for NO_3RR at −1.5 V vs. RHE for ten times; (f) Conceptual electrochemical setup for NH_3 production.

electrocatalyst, we carried out the long-run electrolysis process at −1.5 V which indicated that the catalyst was stable enough for up to 20 h (Fig. 5d). After 20 h, the catalyst showed an ammonia yield rate of 34247.22 μg h^{-1} mg_{cat}^{-1} and FE of 98.62 % at −1.5 V vs RHE. Our result is comparable to other methods (IC method). Recyclability testing is an important factor for practical applications. Ten consecutive recycling tests at −1.5 V was shown in Fig. 5e, and the catalyst showed almost the same NH_3 yield rate and FE, indicating good recyclability during nitrate reduction performance. Fig. S14, which depicts the XRD pattern after electrolysis, demonstrates that the crystalline nature does not change as a result of electrolysis. As a result, the catalyst demonstrates its effectiveness by retaining the structural orientation. After a lengthy electrochemical experiment, FePc's rectangular morphology was seen in the electrocatalyst's microscopic image (Fig. S15). Furthermore, the FePc catalyst is highly selective towards NO_3RR as negligiable amount of by-products[9,63] such as hydrazine and NO_x were formed during the entire experiment (Fig. S18 and S21).

3.5. *Practical applications of NO_3RR in real life*

The manufacturing industry and process sectors have a negative impact on the ecology via pollutants in various forms. As air pollutants, flue gas, green–house gas emissions especially CO_2, accelerates the process of global warming. Secondly, industrial waste water stream

contains toxic water contaminants, among them nitrates are the most notorious one due to their inherent nature of high solubility in water, and it can cause the deadly blue baby syndrome. Hence, to solve the problem, a solution in the shape of conceptual electrochemical setup that will manufacture economically viable ammonia from the nitrates produced by industrial effluents (Fig. 5f). The electrochemical strategy will solve the following issues. First, the ammonia production process involves high temperature and pressure, which leads to massive production of greenhouse gases. Therefore, by using the renewable energy (solar, or wind) powered electrochemical cell ammonia can be produced at ambient conditions, which will drastically cut down CO_2 emissions. Second, ammonia has widespread downstream products with massive utility in the fertilizer sector, and as energy carrier of the future, owing to its high hydrogen storage capacity. Third, it is necessary to convert nitrate exclusively into ammonia, and not into nitrogen oxides (NO_2, NO, etc.) as it is harmful for the environment. The video graphic demonstration (supplementary video 1) of the pH changes in the electrolyte solution from 6 to 12 during NO_3RR further confirms the production of ammonia for practical utility.

Supplementary material related to this article can be found online at doi:10.1016/j.apcatb.2023.123580.

3.6. Theoretical calculation for electronic interaction between Fe & N sites for NO_3 absorption

We performed the DFT calculations to identify active site and the electronic interaction between the metal center as well as different nitrogen coordinated environment for NO_3 absorption on iron phthalocyanine (FePc). The metal center, Fe is more prominent active site to capture the NO_3 molecule, whereas N and C sites are unable to adsorb NO_3 molecule[56]. To unveil the origin of higher NO_3RR selectivity, we studied the electronic properties for NO_3 adsorption. Firstly, we performed the charge density difference analysis to understand the NO_3 adsorption (Fig. 6a-d). The uniform charge redistribution is observed between NO_3 and Fe site and charge of 0.32e is transferred from Fe site to NO_3 during adsorption, which is estimated through bader charge analysis. Similarly, the d band center of Fe atom is studied, which is the well-known electronic descriptor in transition metal systems. It is observed that the value of d band center (–1.48 eV) of Fe site in FePc is shifted towards negative energy (far from Fermi energy level located at 0 eV) after an adsorption of NO_3 and shows the value of −1.95 eV (Fig. 6e-f). These studies confirmed the adsorption of NO_3 on FePc for selective NO_3RR mechanism to synthesis ammonia.

3.7. Reaction mechanism for an in-depth understanding of the interaction of the reactants with active sites

We performed the theoretical computation to investigate the possible mechanism of nitrate reduction reaction (NO_3RR) and catalytic activity on iron phthalocyanine (FePc). The metal center, Fe, is the most dominant active site for capturing the NO_3 molecule, while the N and C sites are incapable of doing so[56]. Here, we considered the FePc model and computed the optimized structures of possible reaction intermediates for NO_3RR, complete reaction mechanism is shown in Fig. 6g.

The mechanism of ammonia synthesis in NO_3RR involves hydrogenation of firstly oxygen and then nitrogen atoms consecutively[64,65]. By considering the energy of each reaction intermediate, we plotted the free energy profile of NO_3RR at U= 0 V to find the potential determining

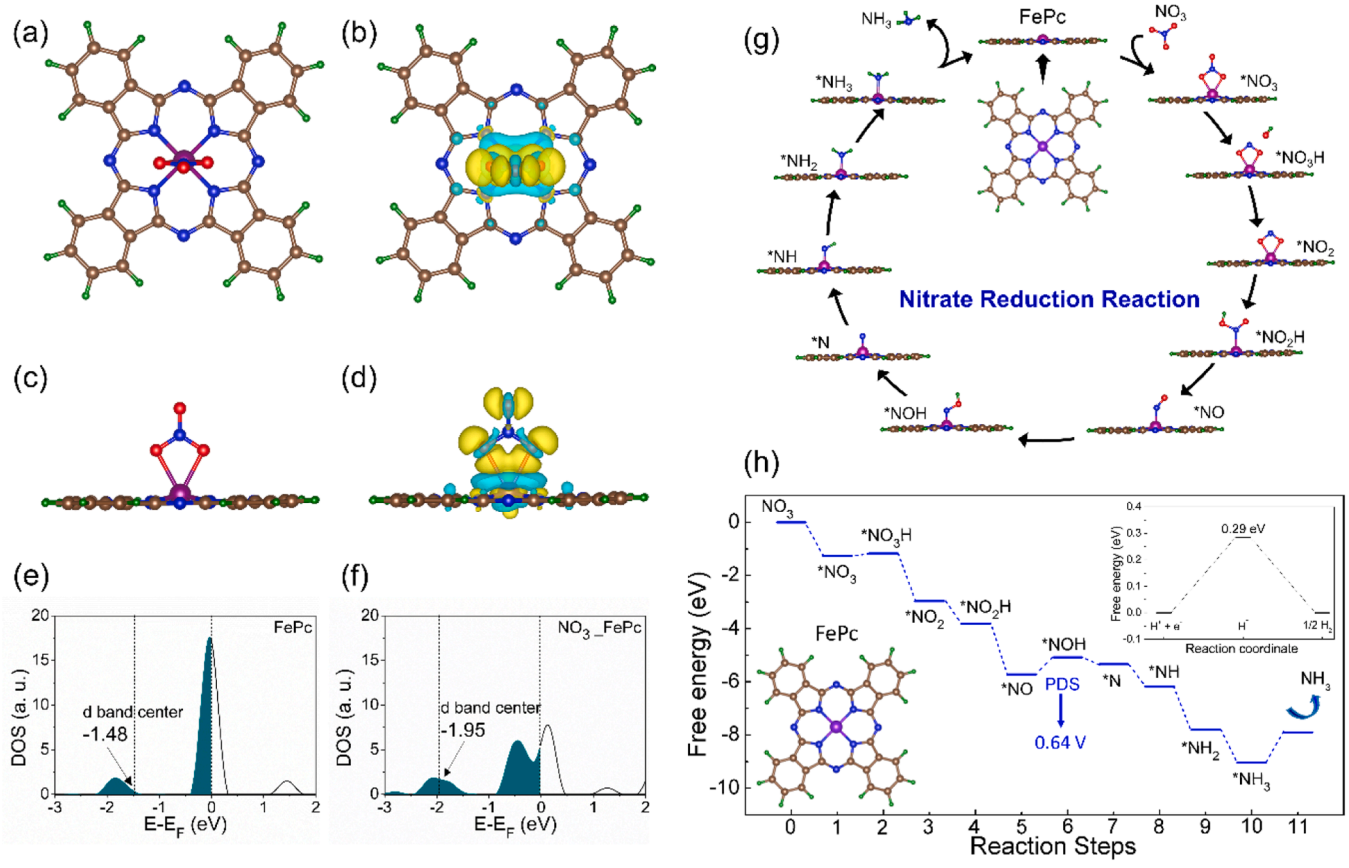

Fig. 6. (a-d) Charge density difference analysis of NO_3 adsorbed FePc catalyst with top and side view; The projected density of state of d orbital of Fe site in (e) FePc and (f) NO_3 adsorbed FePc. The vertical line at 0 eV on X axis represents the Fermi energy level; (g) Shows the reaction mechanism and optimised intermediate structures of nitrate reduction reaction on FePc catalyst. The Fe, N, C, O, H atoms are denoted with pink, blue, gray, red and green color sphere respectively; (h) Free energy profile of nitrate reduction reaction on FePc catalyst. The free energy diagram of hydrogen evolution reaction is given in the subset.

step (PDS) and thermodynamic overpotential (η) (shown in Fig. 6h). Here, we observed that the step *NO to *NOH is the PDS[32] with a value of η is 0.64 V. The last step of release of free NH_3 is not considered as PDS due to high NH_3 solubility[66]. In addition, we also studied the possibility of competitive hydrogen evolution reaction on the on Fe active site of FePc, which can hinder the efficiency of NO_3RR[19,32]. We computed the hydrogen adsorption energy of 0.29 eV on Fe site and observed endothermic nature of H adsorption (inset of the Fig. 6h). Therefore, we confirm that the FePc is more selective for NO_3RR as compared to HER due to stronger (exothermic) adsorption behavior of NO_3 than H respectively. This property remains same for both U= 0 V and U= applied potential. However, a lower PDS value of HER than NO_3RR may cause a slight chance of HER. Also, the H poisoning cannot occur on Fe site because of endothermic nature of H adsorption[67].

4. Conclusions

To conclude, we have designed and developed a novel, rectangular-shaped FePc nanotube electrocatalyst for the selective reduction of nitrate to ammonia under ambient conditions. The chemically synthesized FePc RNTs shows NH_3 yield rate of 35067.09 μg h^{-1} mg_{cat}^{-1} and FE 100 % at −1.5 V for NO_3RR with long term stability. Theoretical computations reveal that the Fe centre is more prominent active site to capture the NO_3 molecule, whereas N and C sites are unable to adsorb NO_3 molecule. The origin of catalytic activity, selectivity and electronic interaction between the metal center and the different nitrogen-coordinated environments toward selective NO_3RR to NH_3 is presented in detail. The local coordination environment of Fe center around pyrrolic and pyridinic N in FePc RNTs is studied by X-ray absorption fine structures (XAFS). The hollow architecture and the Fe-N_4 actives site in FePc are responsible for the outstanding performance of NO_3RR. Finally, video graphic demonstration reveals that the pH change of the electrolyte solution from 6 to 12 during NO_3RR further confirms the production of ammonia in real time. This work sheds significant mechanistic illumination for the tube like hollow framework morphology, the local coordination environment and their interactions in the metal-nitrogen-carbon (M-N-C) based electrocatalyst for selective nitrate reduction to ammonia synthesis.

CRediT authorship contribution statement

Ghorai Uttam Kumar: Conceptualization, Funding acquisition, Project administration, Resources, Supervision, Validation, Visualization, Writing – original draft, Writing – review & editing. **Thapa Ranjit:** Formal analysis, Funding acquisition, Investigation, Resources, Software, Writing – review & editing. **Kapse Samadhan:** Investigation, Resources, Software, Writing – review & editing. **Paul Sourav:** Formal analysis, Investigation, Methodology, Writing – review & editing. **Adalder Ashadul:** Data curation, Formal analysis, Investigation, Methodology, Writing – review & editing. **Sarkar Sougata:** Data curation, Formal analysis, Investigation, Methodology, Writing – original draft.

Declaration of Competing Interest

UKG, SS, AA and SP have filed an Indian Patent application (202131029798) and US patent (US20230279562A1) regarding the electrochemical synthesis of ammonia through nitrogen and nitrate reduction reaction under ambient conditions. The remaining authors declare no competing interests.

Data Availability

Data will be made available on request.

Acknowledgements

AA acknowledges the SERG-CRG for JRF. The authors acknowledge Abharana N., Dr. D. Bhattacharya and Dr. S. N Jha for the XANES experiment. This work is financially supported by SERB (CRG/2022/009427) research grant, WBDSTBT research grant (199 (Sanc.)/ST/P/S&T/6G-12/2018), SERB (CRG/2021/000620) research grant, national supercomputer mission (NSM), India (DST/NSM/R&D_HPC_Applications/2021/19). Authors wish to thank IACS-Kolkata for providing the instrumental facility. The authors thank the High-Performance Computing Center, SRM Institute of Science and Technology for providing computational facilities.

Appendix A. Supporting information

Supplementary data associated with this article can be found in the online version at doi:10.1016/j.apcatb.2023.123580.

References

[1] C.H. Christensen, T. Johannessen, R.Z. Sørensen, J.K. Nørskov, Towards an ammonia-mediated hydrogen economy? Catal. Today 111 (2006) 140–144, https://doi.org/10.1016/J.CATTOD.2005.10.011.
[2] S. Ye, Z. Chen, G. Zhang, W. Chen, C. Peng, X. Yang, L. Zheng, Y. Li, X. Ren, H. Cao, D. Xue, J. Qiu, Q. Zhang, J. Liu, Elucidating the activity, mechanism and application of selective electrosynthesis of ammonia from nitrate on cobalt phosphide, Energy Environ. Sci. 15 (2022) 760–770, https://doi.org/10.1039/D1EE03097C.
[3] S. Paul, A. Adalder, U.K. Ghorai, Progress of electrocatalytic urea synthesis: strategic design, reactor engineering, mechanistic details and techno-commercial study, Mater. Chem. Front. 7 (2023) 3820–3854, https://doi.org/10.1039/D3QM00433C.
[4] D.R. MacFarlane, P.V. Cherepanov, J. Choi, B.H.R. Suryanto, R.Y. Hodgetts, J. M. Bakker, F.M. Ferrero Vallana, A.N. Simonov, A roadmap to the ammonia economy, Joule 4 (2020) 1186–1205, https://doi.org/10.1016/J.JOULE.2020.04.004.
[5] J. Mukherjee, A. Adalder, N. Mukherjee, U.K. Ghorai, Solvothermal synthesis of α–CuPc nanostructures for electrochemical nitrogen fixation under ambient conditions, Catal. Today 423 (2023), 113905, https://doi.org/10.1016/j.cattod.2022.09.011.
[6] Y. Fang, Y. Xue, Y. Li, H. Yu, L. Hui, Y. Liu, C. Xing, C. Zhang, D. Zhang, Z. Wang, X. Chen, Y. Gao, B. Huang, Y. Li, Graphdiyne interface engineering: highly active and selective ammonia synthesis, Angew. Chem. Int. Ed. 59 (2020) 13021–13027, https://doi.org/10.1002/ANIE.202004213.
[7] B.H.R. Suryanto, H.L. Du, D. Wang, J. Chen, A.N. Simonov, D.R. MacFarlane, Challenges and prospects in the catalysis of electroreduction of nitrogen to ammonia, Nat. Catal. 2 (2019) 290–296, https://doi.org/10.1038/s41929-019-0252-4.
[8] X. Liu, Y. Jiao, Y. Zheng, M. Jaroniec, S.Z. Qiao, Building up a picture of the electrocatalytic nitrogen reduction activity of transition metal single-atom catalysts, J. Am. Chem. Soc. 141 (2019) 9664–9672, https://doi.org/10.1021/JACS.9B03811/SUPPL_FILE/JA9B03811_SI_001.PDF.
[9] U.K. Ghorai, S. Paul, B. Ghorai, A. Adalder, S. Kapse, R. Thapa, A. Nagendra, A. Gain, Scalable production of cobalt phthalocyanine nanotubes: efficient and robust hollow electrocatalyst for ammonia synthesis at room temperature, ACS Nano 15 (2021) 5230–5239, https://doi.org/10.1021/ACSNANO.0C10596/ASSET/IMAGES/LARGE/NN0C10596_0006.JPEG.
[10] L. Hui, Y. Xue, H. Yu, Y. Liu, Y. Fang, C. Xing, B. Huang, Y. Li, Highly efficient and selective generation of ammonia and hydrogen on a graphdiyne-based catalyst, J. Am. Chem. Soc. 141 (2019) 10677–10683, https://doi.org/10.1021/JACS.9B03004/SUPPL_FILE/JA9B03004_SI_001.PDF.
[11] S. Murmu, S. Paul, A. Santra, M. Robert, U.K. Ghorai, Graphene wrapped nickel phthalocyanine nanohybrid: Efficient electrocatalyst for nitrogen reduction reaction, Catal. Today 423 (2023), 113938, https://doi.org/10.1016/j.cattod.2022.10.020.
[12] H.L. Du, M. Chatti, R.Y. Hodgetts, P.V. Cherepanov, C.K. Nguyen, K. Matuszek, D. R. MacFarlane, A.N. Simonov, Electroreduction of nitrogen with almost 100% current-to-ammonia efficiency, Nat 609 (2022) 722–727, https://doi.org/10.1038/s41586-022-05108-y.
[13] S. Paul, S. Sarkar, D. Dolui, D. Sarkar, M. Robert, U.K. Ghorai, 1D/2D interface engineering of a CoPc–C 3 N 4 heterostructure for boosting the nitrogen reduction reaction to NH 3, Dalt. Trans. 52 (2023) 15360–15364, https://doi.org/10.1039/D3DT01790G.
[14] R. Zhao, H. Xie, L. Chang, X. Zhang, X. Zhu, X. Tong, T. Wang, Y. Luo, P. Wei, Z. Wang, X. Sun, Recent progress in the electrochemical ammonia synthesis under ambient conditions, EnergyChem 1 (2019), 100011, https://doi.org/10.1016/J.ENCHEM.2019.100011.
[15] A. Adalder, S.R. Waghela, S.A. Shelukar, N. Mukherjee, S. Das, U.K. Ghorai, Carbon black supported manganese phthalocyanine: efficient electrocatalyst for nitrogen

reduction to ammonia, Eng. Rep. (2023), e12705, https://doi.org/10.1002/eng2.12705.
[16] Z. Liang, C. Lee, J. Liu, Y. Hu, D. Han, L. Niu, Q. Yan, Booming electrocatalysts for urea synthesis via nitrogen-integrated carbon dioxide reduction reaction, Mater. Today Catal. 2 (2023), 100011, https://doi.org/10.1016/j.mtcata.2023.100011.
[17] K. Qiu, Y. Han, W. Guo, L. Wang, J. Cheng, Y. Luo, Synthesis of highly twinned ZnSe nanorods for enhancing N2 electrochemical conversion to NH3, Chem. Commun. 59 (2023) 2465–2468, https://doi.org/10.1039/D2CC06776E.
[18] S. Murmu, S. Paul, S. Kapse, R. Thapa, S. Chattopadhyay, A. N, S.N. Jha, D. Bhattacharyya, U.K. Ghorai, Unveiling the genesis of the high catalytic activity in nickel phthalocyanine for electrochemical ammonia synthesis, J. Mater. Chem. A 9 (2021) 14477–14484, https://doi.org/10.1039/D1TA00766A.
[19] G.F. Chen, Y. Yuan, H. Jiang, S.Y. Ren, L.X. Ding, L. Ma, T. Wu, J. Lu, H. Wang, Electrochemical reduction of nitrate to ammonia via direct eight-electron transfer using a copper–molecular solid catalyst, Nat. Energy 5 (2020) 605–613, https://doi.org/10.1038/s41560-020-0654-1.
[20] Y. Wang, C. Wang, M. Li, Y. Yu, B. Zhang, Nitrate electroreduction: mechanism insight, in situ characterization, performance evaluation, and challenges, Chem. Soc. Rev. 50 (2021) 6720–6733, https://doi.org/10.1039/D1CS00116G.
[21] C. Wang, Y. Zhang, H. Luo, H. Zhang, W. Li, W. xian Zhang, J. Yang, Iron-based nanocatalysts for electrochemical nitrate reduction, Small Methods 6 (2022), 2200790, https://doi.org/10.1002/SMTD.202200790.
[22] X. Liang, H. Zhu, X. Yang, S. Xue, Z. Liang, X. Ren, A. Liu, G. Wu, Recent advances in designing efficient electrocatalysts for electrochemical nitrate reduction to ammonia, Small Struct. 4 (2023), 2200202, https://doi.org/10.1002/sstr.202200202.
[23] A. Adalder, S. Paul, U.K. Ghorai, Progress of electrochemical synthesis of nitric acid: catalyst design, mechanistic insights, protocol and challenges, J. Mater. Chem. A. 11 (2023) 10125–10148, https://doi.org/10.1039/D2TA08928A.
[24] S. Zhang, M. Li, J. Li, Q. Song, X. Liu, High-ammonia selective metal-organic framework-derived Co-doped Fe/Fe2O3 catalysts for electrochemical nitrate reduction, Proc. Natl. Acad. Sci. U. S. A. 119 (2022), e2115504119, https://doi.org/10.1073/PNAS.2115504119/SUPPL_FILE/PNAS.2115504119.SAPP.PDF.
[25] S. Paul, S. Sarkar, A. Adalder, S. Kapse, R. Thapa, U.K. Ghorai, Strengthening the metal center of Co–N4 active sites in a 1D–2D heterostructure for nitrate and nitrogen reduction reaction to ammonia, ACS Sustain. Chem. Eng. 11 (2023) 6191–6200, https://doi.org/10.1021/ACSSUSCHEMENG.2C07114.
[26] P. Li, Z. Jin, Z. Fang, G. Yu, A single-site iron catalyst with preoccupied active centers that achieves selective ammonia electrosynthesis from nitrate, Energy Environ. Sci. 14 (2021) 3522–3531, https://doi.org/10.1039/D1EE00545F.
[27] Z.Y. Wu, M. Karamad, X. Yong, Q. Huang, D.A. Cullen, P. Zhu, C. Xia, Q. Xiao, M. Shakouri, F.Y. Chen, J.Y. (Timothy) Kim, Y. Xia, K. Heck, Y. Hu, M.S. Wong, Q. Li, I. Gates, S. Siahrostami, H. Wang, Electrochemical ammonia synthesis via nitrate reduction on Fe single atom catalyst, Nat. Commun. 12 (2021) 1–10, https://doi.org/10.1038/s41467-021-23115-x.
[28] L. Su, F. Zhang, L. Wang, X. Fang, W. Jiang, J. Yang, Flexible electrocatalysts: interfacial-assembly of iron nanoparticles for nitrate reduction, Chem. Commun. 57 (2021) 6740–6743, https://doi.org/10.1039/D1CC02129J.
[29] Li Zhong, Qiru Chen, Haitao Yin, J. Song Chen, Kai Dong, Shengjun Sun, Jun Liu, Haohong Xian, Tingshuai Li, Co 3 O 4 nanoparticles embedded in porous carbon nanofibers enable efficient nitrate reduction to ammonia, Chem. Commun. 59 (2023) 8973–8976, https://doi.org/10.1039/D3CC02023A.
[30] M. Guo, L. Fang, L. Zhang, M. Li, M. Cong, X. Guan, C. Shi, C.L. Gu, X. Liu, Y. Wang, X. Ding, Pulsed electrocatalysis enabling high overall nitrogen fixation performance for atomically dispersed Fe on TiO2, Angew. Chem. Int. Ed. 62 (2023), e202217635, https://doi.org/10.1002/ANIE.202217635.
[31] F.Y. Chen, Z.Y. Wu, S. Gupta, D.J. Rivera, S.V. Lambeets, S. Pecaut, J.Y.T. Kim, P. Zhu, Y.Z. Finfrock, D.M. Meira, G. King, G. Gao, W. Xu, D.A. Cullen, H. Zhou, Y. Han, D.E. Perea, C.L. Muhich, H. Wang, Efficient conversion of low-concentration nitrate sources into ammonia on a Ru-dispersed Cu nanowire electrocatalyst, Nat. Nanotechnol. 17 (2022) 759–767, https://doi.org/10.1038/s41565-022-01121-4.
[32] Y. Wang, W. Zhou, R. Jia, Y. Yu, B. Zhang, Unveiling the activity origin of a copper-based electrocatalyst for selective nitrate reduction to ammonia, Angew. Chem. Int. Ed. 59 (2020) 5350–5354, https://doi.org/10.1002/ANIE.201915992.
[33] Q. Liu, Q. Liu, L. Xie, Y. Ji, T. Li, B. Zhang, N. Li, B. Tang, Y. Liu, S. Gao, Y. Luo, L. Yu, Q. Kong, X. Sun, High-performance electrochemical nitrate reduction to ammonia under ambient conditions using a FeOOH nanorod catalyst, ACS Appl. Mater. Interfaces 14 (2022) 17312–17318, https://doi.org/10.1021/ACSAMI.2C00436/ASSET/IMAGES/LARGE/AM2C00436_0005.JPEG.
[34] Y. Wang, H. Li, W. Zhou, X. Zhang, B. Zhang, Y. Yu, Structurally disordered RuO2 nanosheets with rich oxygen vacancies for enhanced nitrate electroreduction to ammonia, Angew. Chem. Int. Ed. 61 (2022), e202202604, https://doi.org/10.1002/ANIE.202202604.
[35] W. He, J. Zhang, S. Dieckhöfer, S. Varhade, A.C. Brix, A. Lielpetere, S. Seisel, J.R. C. Junqueira, W. Schuhmann, Splicing the active phases of copper/cobalt-based catalysts achieves high-rate tandem electroreduction of nitrate to ammonia, Nat. Commun. 13 (1) (2022) 13, https://doi.org/10.1038/s41467-022-28728-4.
[36] Y. Gao, H. Liu, Z. Zheng, X. Luan, Y. Xue, Y. Li, Controlled growth of a graphdiyne-Prussian blue analog heterostructure for efficient ammonia production (2023), NPG Asia Mater. 151 (15) (2023) 1–10, https://doi.org/10.1038/s41427-022-00439-8.
[37] Y. Li, J. Ma, Z. Wu, Z. Wang, Direct electron transfer coordinated by oxygen vacancies boosts selective nitrate reduction to N2on a Co-CuOx electroactive filter, Environ. Sci. Technol. 56 (2022) 8673–8681, https://doi.org/10.1021/ACS.EST.1C05841/SUPPL_FILE/ES1C05841_SI_001.PDF.
[38] S. Dong, A. Niu, K. Wang, P. Hu, H. Guo, S. Sun, Y. Luo, Q. Liu, X. Sun, T. Li, Modulation of oxygen vacancy and zero-valent zinc in ZnCr2O4 nanofibers by enriching zinc for efficient nitrate reduction, Appl. Catal. B Environ. 333 (2023), 122772, https://doi.org/10.1016/j.apcatb.2023.122772.
[39] A. Adalder, S. Paul, N. Barman, A. Bera, S. Sarkar, N. Mukherjee, R. Thapa, U. K. Ghorai, Controlling the metal–ligand coordination environment of manganese phthalocyanine in 1D–2D heterostructure for enhancing nitrate reduction to ammonia, ACS Catal. 13 (2023) 13516–13527, https://doi.org/10.1021/acscatal.3c02747.
[40] Y. Lan, J. Chen, H. Zhang, W.X. Zhang, J. Yang, Fe/Fe3C nanoparticle-decorated N-doped carbon nanofibers for improving the nitrogen selectivity of electrocatalytic nitrate reduction, J. Mater. Chem. A 8 (2020) 15853–15863, https://doi.org/10.1039/D0TA02317E.
[41] Z. Fang, Z. Jin, S. Tang, P. Li, P. Wu, G. Yu, Porous two-dimensional iron-cyano nanosheets for high-rate electrochemical nitrate reduction, ACS Nano 16 (2022) 1072–1081, https://doi.org/10.1021/ACSNANO.1C08814/ASSET/IMAGES/MEDIUM/NN1C08814_M013.GIF.
[42] H. Xu, J. Wu, W. Luo, Q. Li, W. Zhang, J. Yang, Dendritic cell-inspired designed architectures toward highly efficient electrocatalysts for nitrate reduction reaction, Small 16 (2020), 2001775, https://doi.org/10.1002/SMLL.202001775.
[43] X. Luan, L. Qi, Z. Zheng, S. Zhao, Y. Gao, Y. Xue, Y. Li, In situ growth of a GDY–MnOx heterointerface for selective and efficient ammonia production, Chem. Commun. 59 (2023) 7611–7614, https://doi.org/10.1039/D3CC01428B.
[44] Y. Li, L. Ren, Z. Li, T. Wang, Z. Wu, Z. Wang, Harnessing nickel phthalocyanine-based electrochemical CNT sponges for ammonia synthesis from nitrate in contaminated water, ACS Appl. Mater. Interfaces 14 (2022) 53884–53892, https://doi.org/10.1021/ACSAMI.2C16856/SUPPL_FILE/AM2C16856_SI_001.PDF.
[45] J. Xia, H. Du, S. Dong, Y. Luo, Q. Liu, J.S. Chen, H. Guo, T. Li, Heterogenous Cu@ZrO2 nanofibers enable efficient electrocatalytic nitrate reduction to ammonia under ambient conditions, Chem. Commun. 58 (2022) 13811–13814, https://doi.org/10.1039/D2CC05331D.
[46] F. Xu, L. Zhang, X. Ding, M. Cong, Y. Jin, L. Chen, Y. Gao, Selective electroreduction of dinitrogen to ammonia on a molecular iron phthalocyanine/O-MWCNT catalyst under ambient conditions, Chem. Commun. 55 (2019) 14111–14114, https://doi.org/10.1039/C9CC06574A.
[47] Y. Xue, Q. Yu, Q. Ma, Y. Chen, C. Zhang, W. Teng, J. Fan, W.X. Zhang, Electrocatalytic hydrogenation boosts reduction of nitrate to ammonia over single-atom Cu with Cu(I)-N3C1Sites, Environ. Sci. Technol. 56 (2022) 14797–14807, https://doi.org/10.1021/ACS.EST.2C04456/SUPPL_FILE/ES2C04456_SI_001.PDF.
[48] J. Fan, Y. Chen, X. Chen, Z. Wu, W. Teng, W. Zhang, Atomically dispersed iron enables high-efficiency electrocatalytic conversion of nitrate to dinitrogen on a N-coordinated mesoporous carbon architecture, Appl. Catal. B Environ. 320 (2023), 121983, https://doi.org/10.1016/j.apcatb.2022.121983.
[49] S. Paul, S. Sarkar, A. Adalder, A. Banerjee, U.K. Ghorai, Dual metal site-mediated efficient C–N coupling toward electrochemical urea synthesis, J. Mater. Chem. A. 11 (2023) 13249–13254, https://doi.org/10.1039/D3TA01011B.
[50] J. Mukherjee, S. Paul, A. Adalder, S. Kapse, R. Thapa, S. Mandal, B. Ghorai, S. Sarkar, U.K. Ghorai, Understanding the site-selective electrocatalytic co-reduction mechanism for green urea synthesis using copper phthalocyanine nanotubes, Adv. Funct. Mater. 32 (2022), 2200882, https://doi.org/10.1002/ADFM.202200882.
[51] A. Adalder, S. Paul, B. Ghorai, S. Kapse, R. Thapa, A. Nagendra, U.K. Ghorai, Selective electrocatalytic oxidation of nitrogen to nitric acid using manganese phthalocyanine, ACS Appl. Mater. Interfaces 15 (2023) 34642–34650, https://doi.org/10.1021/acsami.3c01847.
[52] B.W. Dale, R.J.P. Williams, C.E. Johnson, T.L. Thorp, S = 1 spin state of divalent iron. I. Magnetic properties of phthalocyanine iron (II), J. Chem. Phys. 49 (1968) 3441–3444, https://doi.org/10.1063/1.1670617.
[53] P. Coppens, L. Li, N.J. Zhu, Electronic ground state of iron(II) phthalocyanine as determined from accurate diffraction data, J. Am. Chem. Soc. 105 (1983) 6173–6174, https://doi.org/10.1021/JA00357A046/ASSET/JA00357A046.FP.PNG_V03.
[54] J. Bartolomé, C. Monton, I.K. Schuller, Magnetism of metal phthalocyanines, Nanosci. Technol. (2014) 221–245, https://doi.org/10.1007/978-3-642-40609-6_9/COVER.
[55] N. Yan, F. Liu, X. Meng, M. Qin, G. Zhu, L. Bu, Z. Liu, W. Wang, Morphology and structure controls of single-atom Fe–N–C catalysts synthesized using FePc powders as the precursor, Process 9 (2021) 109, https://doi.org/10.3390/PR9010109.
[56] Z.Y. Wu, M. Karamad, X. Yong, Q. Huang, D.A. Cullen, P. Zhu, C. Xia, Q. Xiao, M. Shakouri, F.Y. Chen, J.Y. (Timothy) Kim, Y. Xia, K. Heck, Y. Hu, M.S. Wong, Q. Li, I. Gates, S. Siahrostami, H. Wang, Electrochemical ammonia synthesis via nitrate reduction on Fe single atom catalyst, Nat. Commun. 12 (2021) 1–10, https://doi.org/10.1038/s41467-021-23115-x.
[57] C. He, Z.Y. Wu, L. Zhao, M. Ming, Y. Zhang, Y. Yi, J.S. Hu, Identification of FeN4 as an efficient active site for electrochemical N2 reduction, ACS Catal. 9 (2019) 7311–7317, https://doi.org/10.1021/ACSCATAL.9B00959/ASSET/IMAGES/LARGE/CS-2019-00959E_0004.JPEG.
[58] Y. Wang, L. Zhang, Y. Niu, D. Fang, J. Wang, Q. Su, C. Wang, Boosting NH3 production from nitrate electroreduction via electronic structure engineering of Fe3C nanoflakes, Green. Chem. 23 (2021) 7594–7608, https://doi.org/10.1039/D1GC01913A.
[59] Z. Fang, Z. Jin, S. Tang, P. Li, P. Wu, G. Yu, Porous two-dimensional iron-cyano nanosheets for high-rate electrochemical nitrate reduction, ACS Nano 16 (2022) 1072–1081, https://doi.org/10.1021/ACSNANO.1C08814/SUPPL_FILE/NN1C08814_SI_001.PDF.

[60] W. Haynes, CRC Handbook of Chemistry and Physics - Google Libros, 85, CRC Press, 2014, pp. 4–35. ⟨https://books.google.co.in/books?hl=en&lr=&id=WDll8hA006AC&oi=fnd&pg=PA1&dq=Handbook+of+chemistry+and+physics+by+Lide,+D.+R.+2004&ots=U0oI_QTYMt&sig=_zzDNMtSUTux0JVyK1E5PoXSdUw#v=onepage&q=Handbook of chemistry and physics by Lide%2C D. R. 2004&f=false⟩. accessed February 26, 2023.

[61] P. Gupta, S.S. Das, N.B. Singh, 11 Introduction to spectroscopy. Org. Chem, De Gruyter,, 2022, pp. 205–236, https://doi.org/10.1515/9783110778311-011.

[62] E. Pérez-Gallent, M.C. Figueiredo, I. Katsounaros, M.T.M. Koper, Electrocatalytic reduction of nitrate on copper single crystals in acidic and alkaline solutions, Electrochim. Acta 227 (2017) 77–84, https://doi.org/10.1016/j.electacta.2016.12.147.

[63] P. Saha, S. Amanullah, A. Dey, Electrocatalytic reduction of nitrogen to hydrazine using a trinuclear nickel complex, J. Am. Chem. Soc. 142 (2020) 17312–17317, https://doi.org/10.1021/JACS.0C08785/SUPPL_FILE/JA0C08785_SI_002.CIF.

[64] H. Niu, Z. Zhang, X. Wang, X. Wan, C. Shao, Y. Guo, Theoretical insights into the mechanism of selective nitrate-to-ammonia electroreduction on single-atom catalysts, Adv. Funct. Mater. 31 (2021), 2008533, https://doi.org/10.1002/ADFM.202008533.

[65] Y. Wang, A. Xu, Z. Wang, L. Huang, J. Li, F. Li, J. Wicks, M. Luo, D.H. Nam, C. S. Tan, Y. Ding, J. Wu, Y. Lum, C.T. Dinh, D. Sinton, G. Zheng, E.H. Sargent, Enhanced nitrate-to-ammonia activity on copper-nickel alloys via tuning of intermediate adsorption, J. Am. Chem. Soc. 142 (2020) 5702–5708, https://doi.org/10.1021/JACS.9B13347/ASSET/IMAGES/LARGE/JA9B13347_0004.JPEG.

[66] X. Li, X. Ren, X. Liu, J. Zhao, X. Sun, Y. Zhang, X. Kuang, T. Yan, Q. Wei, D. Wu, A MoS2 nanosheet–reduced graphene oxide hybrid: an efficient electrocatalyst for electrocatalytic N2 reduction to NH3 under ambient conditions, J. Mater. Chem. A 7 (2019) 2524–2528, https://doi.org/10.1039/C8TA10433F.

[67] S. Kapse, S. Narasimhan, R. Thapa, Descriptors and graphical construction for in silico design of efficient and selective single atom catalysts for the eNRR, Chem. Sci. 13 (2022) 10003–10010, https://doi.org/10.1039/D2SC02625B.